

Robustness of quantum critical pairing against disorder

Jian Kang* and Rafael M. Fernandes

School of Physics and Astronomy, University of Minnesota, Minneapolis, MN 55455, USA

The remarkable robustness of high-temperature superconductors against disorder remains a controversial obstacle towards the elucidation of their pairing state. Indeed, experiments report a weak suppression rate of the transition temperature T_c with disorder, significantly smaller than the universal value predicted by extensions of the conventional theory of dirty superconductors. However, in many high- T_c compounds, superconductivity appears near a putative magnetic quantum critical point, suggesting that quantum fluctuations, which suppress coherent electronic spectral weight, may also promote unconventional pairing. Here we investigate theoretically the impact of disorder on such a quantum critical pairing state, considering the coupling of impurities both to the low-energy electronic states and to the pairing interaction itself. We find a significant reduction in the suppression rate of T_c with disorder near the magnetic quantum critical point, shedding new light on the nature of unconventional superconductivity in correlated materials.

I. INTRODUCTION

Elucidating the nature of unconventional superconductivity (SC) remains a major challenge in condensed matter physics. The fact that unconventional SC is found in proximity to a magnetic instability in many heavy-fermion^{1,2}, organic^{3,4}, cuprate⁵, and iron-based compounds⁶, led to the proposal that magnetic fluctuations promote the binding of the electrons in Cooper pairs, resulting in unconventional gap functions that change sign across the Brillouin zone (such as d -wave and s^{+-} -wave gaps)^{7–20}. Indeed, in the phase diagram of high-temperature superconductors such as electron-doped cuprates and iron pnictides, the maximum value of T_c is observed very close to a putative antiferromagnetic (AFM) quantum critical point (QCP)^{21–24}, as shown in Fig. 1. Consequently, the possibility of pairing mediated by quantum critical fluctuations has been extensively investigated recently^{25–34}.

Experimentally, a major tool to probe unconventional SC has been the behavior of T_c with disorder³⁵. In conventional superconductors displaying a s -wave gap, weak non-magnetic impurity scattering is known to be inconsequential to T_c ³⁶, whereas magnetic impurities suppress T_c according to the Abrikosov-Gor'kov (AG) expression³⁷. For a small pair-breaking scattering rate τ^{-1} , AG yields the universal suppression rate $(dT_c/d\tau^{-1})_{AG} = -\pi/4$, confirmed experimentally³⁸ (see Fig. 1). Qualitatively, extensions of the AG theory to d -wave and s^{+-} superconductors reveal that non-magnetic impurities are in general pair-breaking. However, quantitatively, the experimentally observed suppression of T_c with disorder in cuprates and pnictides is rather small compared to the AG-based results^{39–44}. Several scenarios have been proposed to reconcile this robustness of SC against disorder, including strong correlation effects^{52,55}, spatial inhomogeneity of the gap function⁵⁴, spin-fluctuation mediated pairing^{46,53}, disorder-induced enhancement of magnetic fluctuations⁴⁵, distinct intra-orbital and inter-orbital scattering^{47,48,50,51}, and even models advocating for a standard s -wave gap in the pnictides⁵⁶.

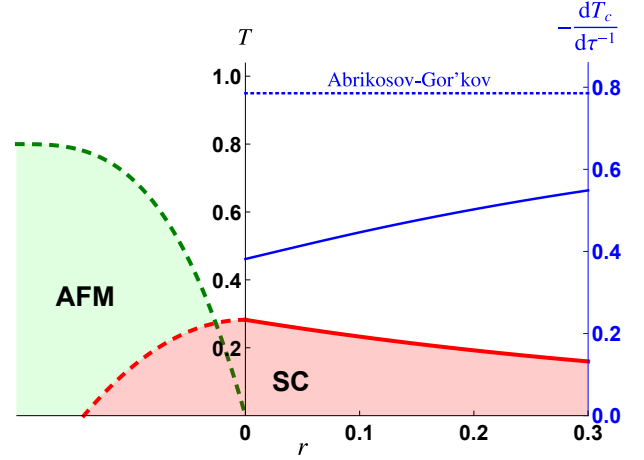


Figure 1. Phase diagram displaying a SC dome near an AFM-QCP. The dashed lines are schematic, whereas the solid lines are the results of our calculations. The red solid line denotes the SC transition temperature of the clean system, T_c , as function of the distance to the QCP, r . Both quantities are in units of the pairing energy scale Λ for a cutoff $\Omega_c = 3\Lambda$ (see text). The blue solid line denotes the suppression rate of T_c with pair-breaking scattering $\tau^{-1} = \tau_Q^{-1}$, $dT_c/d\tau^{-1}$, due to the coupling between disorder and the low-energy electronic states. The blue dotted line is the standard AG universal value $(dT_c/d\tau^{-1})_{AG} = -\pi/4$.

In this paper, to shed light on our understanding of unconventional SC, we focus on how disorder affects critical AFM-mediated pairing beyond the AG paradigm. In particular, we consider the impact of disorder on a general spin-fermion model that describes SC promoted by quantum-critical AFM fluctuations, which can be applied to both cuprates and pnictides. Previously, Ref.⁴⁶ found a strikingly resilient SC state against the effects of disorder near an AFM-QCP. Here, instead of solving the coupled Eliashberg equations⁵⁷, we express them in a convenient functional form^{9,58–60} that allows us to compute directly $dT_c/d\tau^{-1}$ and gain invaluable insight on the different processes by which weak impurity scatter-

ing affects T_c . Specifically, in the limit of weak scattering, three independent contributions arise:

$$\frac{dT_c}{d\tau^{-1}} = \left(\frac{dT_c}{d\tau^{-1}} \right)_f + \left(\frac{dT_c}{d\tau^{-1}} \right)_{b,1} + \left(\frac{dT_c}{d\tau^{-1}} \right)_{b,2} \quad (1)$$

The first term, which yields the results of Fig. 1, arises from the direct coupling of disorder and the low-energy electronic states. This coupling leads to a decrease of the electronic coherent spectral weight near the QCP, which in turn suppresses the reduction of the pairing vertex caused by pair-breaking scattering, in agreement with the general results from Ref.⁴⁶. In particular, at the QCP, we find the value $\left(\frac{dT_c}{d\tau^{-1}} \right)_f \approx -0.45$, which is about half of the value expected from AG theory. The last two terms in the equation above arise from the coupling of disorder and the bosonic degrees of freedom that promote the pairing interaction – in this case, spin fluctuations. In general, $\left(\frac{dT_c}{d\tau^{-1}} \right)_{b,2} < 0$ comes from the suppression of the correlation length of the quantum critical fluctuations by disorder. On the other hand, $\left(\frac{dT_c}{d\tau^{-1}} \right)_{b,1} > 0$ appears due to the renormalization of the electron-boson vertex, and is generally larger than $\left| \left(\frac{dT_c}{d\tau^{-1}} \right)_{b,2} \right|$. Consequently, the impact of disorder on the pairing interaction leads to an additional reduction of $dT_c/d\tau^{-1}$ with respect to the AG value. Our results offer a fresh perspective on the robustness of unconventional SC against disorder, lending support to the proposal that quantum critical pairing plays an important role in copper- and iron-based SC.

The paper is organized as follows: Section II introduces the spin-fermion model and the SC gap equations. Section III discusses the coupling between disorder and the fermionic degrees of freedom, which yields $\left(\frac{dT_c}{d\tau^{-1}} \right)_f$, whereas Section IV discusses the coupling between disorder and the bosonic degrees of freedom, which yields $\left(\frac{dT_c}{d\tau^{-1}} \right)_{b,1}$ and $\left(\frac{dT_c}{d\tau^{-1}} \right)_{b,2}$. Section V is devoted to the concluding remarks. Analytical approximations to $\left(\frac{dT_c}{d\tau^{-1}} \right)_{b,1}$ and $\left(\frac{dT_c}{d\tau^{-1}} \right)_{b,2}$ are given in Appendix A.

II. SPIN-FERMION MODEL AND THE LINEARIZED GAP EQUATIONS

Our starting point is the low-energy spin-fermion model, in which electrons couple to a bosonic AFM order parameter ϕ_q , whose fluctuations are described by the magnetic susceptibility $\chi_b(\mathbf{q}, \Omega_n)$. We focus on the electronic states $c_{\mathbf{k}\sigma}$ and $d_{\mathbf{k}\sigma} \equiv c_{\mathbf{k}+\mathbf{Q}\sigma}$ in the vicinities of a pair of hot spots, i.e. points of the Fermi surface connected by the AFM ordering vector \mathbf{Q} . The action is given by^{26,46}:

$$S = \int_{\mathbf{k}} (-i\omega_n + \epsilon_c(\mathbf{k})) c_{\mathbf{k}\sigma}^\dagger c_{\mathbf{k}\sigma} + \int_{\mathbf{k}} (-i\omega_n + \epsilon_d(\mathbf{k})) d_{\mathbf{k}\sigma}^\dagger d_{\mathbf{k}\sigma} + \lambda \int_{\mathbf{k}, \mathbf{q}} \phi_{-\mathbf{q}} \cdot \left(c_{\mathbf{k},\alpha}^\dagger \boldsymbol{\sigma}_{\alpha\beta} d_{\mathbf{k}+\mathbf{q},\beta} \right) + \int_{\mathbf{q}} \chi_b^{-1}(\mathbf{q}, \Omega_n) \phi_{\mathbf{q}} \cdot \phi_{-\mathbf{q}} \quad (2)$$

where $\int_{\mathbf{k}} = T \sum_n \int \frac{d^d k}{(2\pi)^d}$, λ is the coupling constant, $\epsilon_d(\mathbf{k}) \equiv \epsilon_c(\mathbf{k} + \mathbf{Q})$, and $\omega_n = (2n+1)\pi T$ is the fermionic Matsubara frequency. Because the behavior of this action is dominated by the states near the hot spots²⁸, we linearize the spectrum near them, $\epsilon_c(\mathbf{k}) \approx \mathbf{v}_c \cdot \mathbf{k}$ and $\epsilon_d(\mathbf{k}) \approx \mathbf{v}_d \cdot \mathbf{k}$, where \mathbf{k} is measured with respect to the Fermi momentum. Thus, by focusing on a single pair of hot spots, this model can in principle be applied to either cuprates or pnictides. Indeed, as shown in Fig. 2, there are four pairs of hot spots in the typical Fermi surface of the cuprates (in which $\mathbf{Q} = (\pi, \pi)$) and eight for the iron pnictides (in which $\mathbf{Q} = (\pi, 0)$ or $(0, \pi)$). Hereafter, for simplicity, we consider the special case $|\mathbf{v}_c| = |\mathbf{v}_d|$, but the main results should remain valid otherwise.

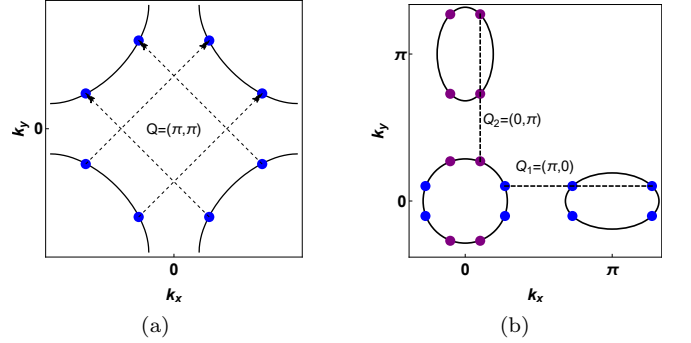


Figure 2. Schematic Fermi surfaces of (a) the cuprates and (b) iron pnictides, respectively. Pairs of hot spots (blue or purple points) are connected by dashed lines, corresponding to the momentum $\mathbf{Q} = (\pi, \pi)$, for the cuprates, and $\mathbf{Q} = (\pi, 0)$ or $(0, \pi)$, for the pnictides. Spin fluctuations are peaked at these wave-vectors in the two materials.

For such a low-energy model, the magnetic susceptibility can be expanded as $\chi_b^{-1}(\mathbf{q}, \Omega_n) = \chi_0^{-1}(r_0 + q^2 + \Omega_n^2/v_b^2)$, where χ_0^{-1} is the magnetic energy scale determined by high-energy states, r_0 is the distance to the bare AFM quantum critical point, and v_b is the spin-wave velocity. The coupling to the electronic degrees of freedom, however, fundamentally changes this propagator by introducing Landau damping, i.e. the decay of magnetic excitations in electron-hole pairs. Within one-loop, the renormalized magnetic susceptibility becomes $\chi^{-1} = \chi_b^{-1} - \Pi(\mathbf{q}, \Omega_n)$, where Π is the standard Lindhard function. Expanding it for small momentum and frequency, we find:

$$\chi(\mathbf{q}, \Omega_n) = \frac{\chi_0}{\xi^{-2} + \mathbf{q}^2 + |\Omega_n|/\gamma}, \quad (3)$$

where $\xi^{-2} = r_0 - \chi_0 \Pi(0, 0)$ is the inverse squared correlation length, which vanishes at the QCP, and $\gamma^{-1} = \lambda^2 \chi_0 / (2\pi v_F^2 \sin \theta)$ is the Landau damping. Experimentally, the distance to the QCP can be accessed by the NMR spin-lattice relaxation rate, since $T_1 T \propto \xi^{-2}$ for a quasi-2D system. Here, θ is the angle between \mathbf{v}_c and \mathbf{v}_d . To complete the model, we introduce the contributions

from the small-momentum and large-momentum impurity potentials, u_0 and u_Q respectively:

$$S_{\text{imp}} = \int_{kk'} u_0 (c_{\mathbf{k}\sigma}^\dagger c_{\mathbf{k}'\sigma} + d_{\mathbf{k}\sigma}^\dagger d_{\mathbf{k}'\sigma}) + \int_{kk'} u_Q (c_{\mathbf{k}\sigma}^\dagger d_{\mathbf{k}'\sigma} + h.c.) \quad (4)$$

For a point-like impurity, such as considered in Ref.⁴⁶, it follows that $u_0 = u_Q$.

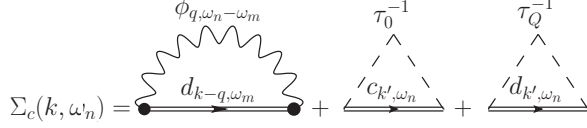


Figure 3. Feynman diagrams for the fermionic self-energy Σ , including the fermion-boson coupling and disorder scattering.

The spin-fermion model (2) has been studied by a variety of different techniques, from large- N ^{26,27} and RG^{66,67} to Quantum Monte Carlo²⁸. Here, we consider the large- N approach, where N is the number of hot spots. Its main advantage is that it allows one to set up an Eliashberg-like approach to compute T_c . This is because, as shown in Ref.²⁶, the vertex corrections are suppressed by the factor $1/N$ and, thus, the SC gap equations can be obtained by evaluating the one-loop self-energy shown in Fig. 3. The normal component of the self-energy has a real part Σ' , which can be absorbed as a renormalization of the band dispersion, and an imaginary part Σ'' , which gives rise to a frequency-dependent fermionic coherent spectral weight Z_n^{-1} according to $Z_n = 1 - \Sigma''/\omega_n$. The anomalous component of the self-energy, W_n , is proportional to the frequency-dependent SC gap, $\Delta_n = W_n/Z_n$.

Spin fluctuations promote attraction in the SC channel in which the gap changes sign from one hot spot to another, i.e. $W_n^c = -W_n^d \equiv W_n$, corresponding to either a d -wave gap or an s^{+-} gap, depending on the position of the hot spots in the Brillouin zone (see Fig. 2). In the Nambu spinor representation, the fermionic self energy is in the form⁹:

$$\Sigma(i\omega_n, \mathbf{k}) = i\omega_n(1 - Z_n)\sigma_0 + \zeta\sigma_3 + W_n\sigma_1, \quad (5)$$

where σ_i are Pauli matrices. In principle, both Z_n and W_n depend on the momentum \mathbf{k} . In our approach, where only pairs of hot spots are considered, the momentum dependence is neglected and only the frequency dependence is considered. We note that, as discussed in Refs.^{27,31}, the contributions from states beyond the hot spots can give rise to important effects. However, in what concerns the linearized gap equations, these effects become important when the energy scale associated with the curvature of the Fermi surface is comparable to T_c (see Ref.³¹). Therefore, our approach is suitable for Fermi surfaces whose curvatures are small. In this case, the fermionic Green's function is given by:

$$G^{-1}(i\omega_n, \mathbf{k}) = i\omega_n Z_n - \epsilon\sigma_3 - W_n\sigma_1 \\ \Rightarrow G(i\omega_n, \mathbf{k}) = -\frac{i\omega_n Z_n + \epsilon\sigma_3 + W_n\sigma_1}{(Z_n\omega_n)^2 + \epsilon^2 + W_n^2}, \quad (6)$$

where we absorbed the real-part of the normal self-energy ζ in the electronic dispersion ϵ .

By computing the one-loop self-energy in Fig. 3, the linearized Eliashberg equations ($T = T_c$) in the presence of disorder can be written as

$$i\omega_n(1 - Z_{n,c}(\mathbf{k})) = 3\lambda^2 T \sum_m \int \frac{d^2 q}{(2\pi)^2} \frac{\chi_0}{\xi^{-2} + q^2 + |\omega_n - \omega_m|/\gamma} \frac{-i\omega_m Z_{m,d}}{(\omega_m Z_{m,d})^2 + \epsilon_d^2(\mathbf{k} - \mathbf{q})} - i \frac{\text{sgn}(\omega_n)}{2\tau} \quad (7)$$

$$W_{n,c}(\mathbf{k}) = T \sum_m \int \frac{d^2 q}{(2\pi)^2} \frac{-3\lambda^2 \chi_0}{\xi^{-2} + q^2 + \frac{|\omega_n - \omega_m|}{\gamma}} \frac{W_{m,d}}{(\omega_m Z_{m,d})^2 + \epsilon_d^2(\mathbf{k} - \mathbf{q})} + \frac{(2\tau_0)^{-1} W_{n,c}}{|\omega_n| Z_{n,c}} + \frac{(2\tau_Q)^{-1} W_{n,d}}{|\omega_n| Z_{n,d}} \quad (8)$$

The subscripts c, d refer to the fermionic states around the two hot spots. The equations for $Z_{n,d}$ and $W_{n,d}$ assume similar forms. The total impurity scattering rate is given by $\tau^{-1} = \tau_0^{-1} + \tau_Q^{-1}$, where $\tau_0^{-1} = 2\pi n_{\text{imp}} u_0^2 N_f$ is the small-momentum scattering rate and $\tau_Q^{-1} = 2\pi n_{\text{imp}} u_Q^2 N_f$ is the large-momentum scattering rate, with n_{imp} denoting the concentration of impurities and N_f , the density of states at the Fermi level. Both Eqs. (7) and (8) contain the two-dimensional integral over momenta q_{\parallel} and q_{\perp} , i.e. the components of \mathbf{q} parallel and perpendicular to the Fermi surface. Focusing at

the hot spot ($\mathbf{k} = 0$), the fermionic self-energy is

$$\int \frac{d^2 q}{(2\pi)^2} \frac{\chi_0}{\xi^{-2} + q^2 + |\omega_n - \omega_m|/\gamma} \frac{-i\omega_m Z_{m,d}}{(\omega_m Z_{m,d})^2 + \epsilon_d^2(\mathbf{q})} \\ = \int \frac{dq_{\perp}}{(2\pi)} \frac{\chi_0/2}{\sqrt{\xi^{-2} + q_{\perp}^2 + |\omega_n - \omega_m|/\gamma}} \frac{-i\omega_m Z_{m,d}}{(\omega_m Z_{m,d})^2 + (v_f q_{\perp})^2} \\ \approx \frac{\chi_0}{4v_f} \frac{-i\text{sgn}(\omega_m)}{\sqrt{\xi^{-2} + |\omega_n - \omega_m|/\gamma}}. \quad (9)$$

where, in the last step, we considered that:

$$\xi^{-2} + |\omega_n - \omega_m|/\gamma \gg \left(\frac{\omega_m Z_m}{v_f} \right)^2 \quad (10)$$

which naturally establishes a cutoff:

$$\Omega_c = \max\left(\frac{v_f^2}{\gamma}, \frac{v_f}{\xi}\right) = \max\left(\frac{8\Lambda}{9\pi \sin^2 \theta}, \frac{4\sqrt{r}\Lambda}{3 \sin \theta}\right) \quad (11)$$

where $r = \frac{\xi^{-2}\gamma}{2\pi}$ is the energy scale of the AFM fluctuations, and $\Lambda = \frac{9}{16}\lambda^2\chi_0 \sin \theta$ is an effective coupling constant. Note that this cutoff arises not from the bandwidth, but from the restriction in the momentum integration. For notation convenience, we define

$$A(\omega_n - \omega_m) = \frac{\chi_0}{2\sqrt{\xi^{-2} + |\omega_n - \omega_m|/\gamma}} \quad (12)$$

Therefore, the Eliashberg equations are given by:

$$Z_n = 1 + \frac{3\lambda^2 T}{2v_f \omega_n} \sum_m \text{sgn}(\omega_m) A(\omega_n - \omega_m) + \frac{\tau_0^{-1} + \tau_Q^{-1}}{2|\omega_n|} \quad (13)$$

$$W_n = \frac{3\lambda^2 T}{2v_f} \sum_m \frac{W_m}{Z_m} A(\omega_n - \omega_m) + \frac{W_n (\tau_0^{-1} - \tau_Q^{-1})}{2|\omega_n| Z_n} \quad (14)$$

Our goal is to investigate how $dT_c/d\tau^{-1}$ deviates from the universal AG result, $(dT_c/d\tau^{-1})_{\text{AG}} = -\pi/4$. To gain insight into this problem, we reexpress the Eliashberg equations as a functional form^{9,58–60}. In particular, after defining $\bar{\Delta}_n = TW_n/(Z_n|\omega_n|)$ and restricting the solution to even-frequency pairing, $W(-\omega_n) = W(\omega_n)$, solving the Eliashberg equations becomes equivalent to finding the zero eigenvalue η of $\hat{K}_{mn}\bar{\Delta}_n = \eta\bar{\Delta}_m$. Here, the matrix \hat{K} is given by:

$$\begin{aligned} \hat{K}_{m \neq n} &= \sqrt{\frac{\Lambda}{T}} \left(\frac{1}{\sqrt{|m-n|+r/T}} + \frac{1}{\sqrt{m+n+1+r/T}} \right) \\ \hat{K}_{nn} &= \sqrt{\frac{\Lambda}{T}} \frac{1}{\sqrt{2n+1+r/T}} - \pi(2n+1) \\ &\quad - \sqrt{\frac{\Lambda}{T}} \sum_{n' \neq n} \frac{\text{sgn}(\omega_{n'})}{\sqrt{|n-n'|+r/T}} - \frac{\tau_Q^{-1}}{T} \end{aligned} \quad (15)$$

where m, n are non-negative integers. T_c is obtained when the largest eigenvalue η vanishes. These equations reduce to those studied in Ref.⁴⁶ when $\tau_0^{-1} = \tau_Q^{-1}$. The main advantage of this functional approach is that it allows us to study the impact of weak disorder on T_c without having to solve explicitly the disordered equations. This is accomplished by employing the Hellmann-Feynman theorem:

$$\frac{dT_c}{d\tau^{-1}} = - \left\langle \frac{d\hat{K}}{d\tau^{-1}} \right\rangle / \left\langle \frac{d\hat{K}}{dT_c} \right\rangle \equiv - \left(\frac{d\eta}{d\tau^{-1}} \right) / \left(\frac{d\eta}{dT_c} \right) \quad (16)$$

where $\langle \dots \rangle$ refers to an average with respect to the normalized eigenvector $\bar{\Delta}_n$ of the system without disorder and $\eta = \sum_{m,n} \hat{K}_{mn} \bar{\Delta}_m \bar{\Delta}_n$. Next, we divide the contributions to $(dT_c/d\tau^{-1})$ in two classes: those arising from

the coupling between disorder and the fermionic degrees of freedom, $(\frac{dT_c}{d\tau^{-1}})_{f,i}$, and those arising from the coupling between disorder and the bosonic degrees of freedom (i.e. the pairing interaction), $(\frac{dT_c}{d\tau^{-1}})_{b,j}$. While the former corresponds simply to the τ_Q^{-1} term in Eq. (15), the latter is implicit in the kernel (15) via the dependence of the pairing interaction $A(\Omega_n)$ on disorder. Because of Hellmann-Feynman theorem, these contributions can be treated independently and just added up in the end:

$$\frac{dT_c}{d\tau^{-1}} = \sum_i \left(\frac{dT_c}{d\tau^{-1}} \right)_{f,i} + \sum_j \left(\frac{dT_c}{d\tau^{-1}} \right)_{b,j} \quad (17)$$

III. SUPPRESSION OF T_c DUE TO THE COUPLING OF DISORDER AND THE ELECTRONIC DEGREES OF FREEDOM

We first investigate how the coupling between disorder and the fermionic states affects the suppression rate $(\frac{dT_c}{d\tau^{-1}})$. As it is immediate clear from Eq. (15), there is only one term in the kernel that depends on the impurity scattering explicitly, giving rise to the contribution $(\frac{dT_c}{d\tau^{-1}})_f$. In particular, because only the large-momentum scattering rate τ_Q^{-1} appears in the functional \hat{K} , T_c is insensitive to small-momentum scattering τ_0^{-1} – an extension of the Anderson theorem to sign-changing SC gaps. Before we numerically evaluate (16), it is instructive to consider two limiting cases: the BCS limit and quantum critical pairing.

A. BCS Limit

The BCS limit corresponds to the case in which the system is far away from the QCP and the coupling constant is small, $r \gg \Omega_c \gg \Lambda$. The pairing interaction then becomes frequency-independent and small, $A(\Omega_n) \propto r^{-1/2}$, and the fermionic coherence factor can be approximated by $Z_n \approx 1$. In this limit, Eq. (15) becomes

$$\begin{aligned} K_{mn} &\approx 2\sqrt{\frac{\Lambda}{r}} - \pi(2n+1)\delta_{mn} \implies \\ \bar{\Delta}_{n \geq 0} &= \frac{2}{\pi(2n+1)} \sqrt{\frac{\Lambda}{r}} \sum_{m \leq \frac{\Omega_c}{2\pi T}} \bar{\Delta}_m \end{aligned} \quad (18)$$

Defining the quantity $c = \sum_m \bar{\Delta}_m$, we obtain the self-consistent equation:

$$\begin{aligned} c &= \frac{c}{\pi} \sqrt{\frac{\Lambda}{r}} \sum_{n \leq \Omega_c/(2\pi T)} \frac{1}{n + 1/2} \\ &= \frac{c}{\pi} \sqrt{\frac{\Lambda}{r}} \left[\psi\left(\frac{\Omega_c}{2\pi T} - \frac{1}{2}\right) - \psi\left(\frac{1}{2}\right) \right] \\ \Rightarrow T_c &\approx \frac{\Omega_c}{2\pi} \exp \left[-\pi \sqrt{\frac{r}{\Lambda}} - \psi\left(\frac{1}{2}\right) \right] \end{aligned} \quad (19)$$

which agrees with the standard BCS expression. Here, $\psi(x)$ is the digamma function.

As shown in Eq. (18), the matrix elements of \hat{K} are independent of T , but the eigenvalue η still depends on T via the changes in the matrix size N_c , which is set by the hard cutoff Ω_c via $N_c = \Omega_c/(2\pi T)$. To take this effect into account, consider a reduction in the matrix size by 1, $N_c \rightarrow N_c - 1$, which means that the last row and the last column no longer take part in the determination of the eigenvalue. Then, the change in $\eta = \sum_{m,n} \hat{K}_{mn} \bar{\Delta}_m \bar{\Delta}_n$ is given by:

$$\begin{aligned} \delta\eta &= - \sum_m \left(\hat{K}_{mN_c} + \hat{K}_{N_c m} \right) \bar{\Delta}_m \bar{\Delta}_{N_c} + \hat{K}_{N_c N_c} (\bar{\Delta}_{N_c})^2 \\ &= \hat{K}_{N_c N_c} (\bar{\Delta}_{N_c})^2 \end{aligned} \quad (20)$$

Therefore, we find:

$$\frac{\delta\eta}{\delta T_c} = - \frac{\Omega_c}{2\pi T^2} \frac{\delta\eta}{\delta N_c} = \frac{\Omega_c}{2\pi T^2} \hat{K}_{N_c N_c} (\bar{\Delta}_{N_c})^2 \quad (21)$$

yielding:

$$\begin{aligned} \frac{dT_c}{d\tau_Q^{-1}} &= - \left(\frac{d\eta}{dT_c} \right)^{-1} \frac{d\eta}{d\tau_Q^{-1}} \\ &= \frac{1}{N_c} \frac{1}{\hat{K}_{N_c N_c} (\bar{\Delta}_{N_c})^2} \end{aligned} \quad (22)$$

Using Eq. (18), we have $\hat{K}_{N_c N_c} = -\pi(2N_c + 1) \approx -2\pi N_c$. Furthermore, from the same equation, we have:

$$\bar{\Delta}_{N_c} = \frac{c}{\pi(N_c + \frac{1}{2})} \sqrt{\frac{\Lambda}{r}} \quad (23)$$

where $c = \sum_{m \leq \frac{\Omega_c}{2\pi T}} \bar{\Delta}_m$. The value of c can be obtained by normalizing the eigenvector:

$$\sum_{n=0}^{\frac{\Omega_c}{2\pi T}} \bar{\Delta}_n^2 = 1 \quad \Rightarrow \quad \frac{c}{\pi} \sqrt{\frac{\Lambda}{r}} = \left(\sum_n \frac{1}{(n + 1/2)^2} \right)^{-1/2} \quad (24)$$

Therefore:

$$\begin{aligned} \bar{\Delta}_{N_c} &= \frac{1}{N_c + 1/2} \left(\sum_n \frac{1}{(n + 1/2)^2} \right)^{-1/2} \approx \frac{\sqrt{2}}{\pi N_c} \\ \Rightarrow \frac{dT_c}{d\tau_Q^{-1}} &\approx - \frac{1}{N_c} \frac{1}{2\pi N_c} \left(\frac{\pi N_c}{\sqrt{2}} \right)^2 = - \frac{\pi}{4}. \end{aligned} \quad (25)$$

recovering the Abrikosov-Gor'kov universal value for dirty superconductors.

B. Quantum Critical Pairing Limit

The second limiting case corresponds to the system at the QCP, for which $r \propto \xi^{-2} = 0$. In this case, the pairing interaction is strongly frequency-dependent, $A(\Omega_n) \propto \Omega_n^{-1/2}$. From Eq. (13), we find that as $T \rightarrow 0$ the low-frequency coherent factor vanishes as $Z^{-1}(\omega \ll \Omega_c) \propto \omega^{1/2}$, a hallmark of non-Fermi liquid behavior. An interesting property of the system of equations at the QCP is that they converge in the limit $\Omega_c \rightarrow \infty$, i.e. T_c and $(\frac{dT_c}{d\tau_Q^{-1}})$ do not depend on the cutoff. In this limit, the \hat{K} matrix becomes:

$$\begin{aligned} \hat{K}_{nn} &= \frac{\sqrt{\Lambda/T}}{\sqrt{2n+1}} - \pi(2n+1) - \frac{1}{\tau_Q T} \\ &\quad - 2\sqrt{\frac{\Lambda}{T}} \left[\zeta\left(\frac{1}{2}, 1\right) - \zeta\left(\frac{1}{2}, n+1\right) \right] \end{aligned} \quad (26)$$

$$\hat{K}_{m \neq n} = \sqrt{\frac{\Lambda}{T}} \left(\frac{1}{\sqrt{|n-m|}} + \frac{1}{\sqrt{n+m+1}} \right). \quad (27)$$

where $\zeta(\frac{1}{2}, x)$ is the Hurwitz zeta function. Clearly, the only free parameter is the combination $\frac{\Lambda}{T_c}$. By numerically diagonalizing the matrix, we find $T_c \approx 0.5\Lambda$. Analysis of the eigenvalue problem for large frequencies reveal that $\bar{\Delta}_n \propto n^{-3/2}$, which explains why the problem converges for $\Omega_c \rightarrow \infty$. This is to be contrasted with the BCS case, in which $\bar{\Delta}_n \propto n^{-1}$, implying that the sum does not converge and a cutoff is needed.

To compute $(\frac{dT_c}{d\tau_Q^{-1}})$, we use the Hellmann-Feynman theorem, Eq. (16). Using the equations above, we find:

$$\frac{\partial \hat{K}_{mn}}{\partial \tau_Q^{-1}} = 0 \quad \frac{\partial \hat{K}_{mn}}{\partial \tau_Q^{-1}} = -\delta_{mn}/T \quad (28)$$

and:

$$\frac{\partial \hat{K}_{mn}}{\partial T} = -\frac{\hat{K}_{mn}}{2T} - \frac{\pi(2n+1)}{2T} \delta_{mn} \quad (29)$$

Hence, we obtain:

$$\begin{aligned} \left(\frac{d\eta}{dT} \right) &= -\frac{\pi}{2T} \sum_{n=0}^{\infty} \bar{\Delta}_n^2 (2n+1) \\ \Rightarrow \frac{dT_c}{d\tau_Q^{-1}} &= -\frac{2}{\pi} \left(\sum_{n=0}^{\infty} \bar{\Delta}_n^2 (2n+1) \right)^{-1} \end{aligned} \quad (30)$$

The term inside the brackets does not depend on any free parameters, and therefore can be evaluated numerically. Numerical evaluation gives $dT_c/d\tau_Q^{-1} \approx -0.45$, which is smaller than the AG universal value obtained away from the QCP.

C. General case

Therefore, the two limiting cases ($r = 0$ and $r \gg \Omega_c \gg \Lambda$) suggest that proximity to the QCP promotes the robustness of T_c against pair-breaking disorder. Before presenting the results for a general distance r from the QCP, we first explain how the high-energy cutoff Ω_c is set in our calculation. In the subsection discussing the BCS limit, we set a hard cutoff $N_c = \Omega_c / (2\pi T)$ in the Matsubara sum. Although this procedure does not affect the behavior of T_c in the limit of $\Omega_c \gg T_c$, it will make T_c behave discontinuously as Ω_c and r decrease. To avoid such a discontinuity, we set instead a soft cutoff in the Matsubara sum by including an appropriate continuous function $f(\omega_n)$ that is strongly suppressed above Ω_c and nearly 1 below Ω_c . Specifically, we change the bosonic propagator to:

$$\frac{1}{|\omega_n - \omega_m|/\gamma + \mathbf{q}^2 + \xi^{-2}} \rightarrow \frac{f(\omega_n)f(\omega_m)}{|\omega_n - \omega_m|/\gamma + \mathbf{q}^2 + \xi^{-2}} \quad (31)$$

with $f(\omega) = \left[\exp\left(\frac{|\omega| - \Omega_c}{\Lambda_d}\right) + 1 \right]^{-1}$, where $\Lambda_d = 0$ gives the hard energy cutoff. This function has the property that when $|\omega| \ll \Omega_c$, $f(\omega) \approx 1$, and when $|\omega| \gg \Omega_c$, $f(\omega) \approx 0$. In our calculation, Λ_d is set to be $\Lambda_d = \max(0.1\Lambda, 0.3\Omega_c)$. We emphasize that none of our results qualitatively change for $\Lambda_d = 0$ or Λ_d small. Thus, at the QCP, the matrix \hat{K} with such soft high-energy cutoff becomes:

$$\hat{K}_{m \neq n} = \sqrt{\frac{\Lambda}{T}} \left(\frac{f_m f_n}{\sqrt{|n-m| + r/T}} + \frac{f_m f_n}{\sqrt{n+m+1 + r/T}} \right) \quad (32)$$

$$\begin{aligned} \hat{K}_{nn} = & f_n^2 \sqrt{\frac{\Lambda}{(2n+1)T + r}} - \pi(2n+1) \\ & - f_n \sqrt{\frac{\Lambda}{T}} \sum_{m \neq n} \frac{\text{sgn}(\omega_m) f_m}{\sqrt{|n-m| + r/T}} - \frac{1}{\tau_Q T} \end{aligned} \quad (33)$$

where

$$f_{n \geq 0} = f(\pi(2n+1)T) \quad (34)$$

is the weight function. In the clean limit ($\tau_Q^{-1} = 0$), it is straightforward to compute T_c by diagonalizing the matrix \hat{K} . As shown in Fig. III C, we find that T_c is generally suppressed away from the QCP for a fixed value of the cutoff Ω_c .

We are now in position to compute the suppression rate of T_c by disorder using the Hellmann-Feynman theorem, Eq. (16), combined with the solution of the clean system discussed above. From Eqs. (32) and (33), we have $\partial \hat{K} / \partial \tau_Q^{-1} = 0$, and $\partial \hat{K} / \partial \tau_Q^{-1} = -1/T$, i.e. only large-momentum scattering is pair-breaking. Since we apply the soft cutoff here, the weight function f also depends on temperature, as shown by Eq. (34). We have:

$$\begin{aligned} \frac{\partial \hat{K}_{m \neq n}}{\partial T} = & -\frac{\pi}{\Lambda_d} \sqrt{\frac{\Lambda}{T}} f_m f_n \left((2n+1)(1-f_n) + (2m+1)(1-f_m) \right) \left(\frac{1}{\sqrt{|n-m| + r/T}} + \frac{1}{\sqrt{n+m+1 + r/T}} \right) \\ & + \frac{r}{2T^2} \sqrt{\frac{\Lambda}{T}} f_m f_n \left[(|n-m| + r/T)^{-\frac{3}{2}} + (n+m+1 + r/T)^{-\frac{3}{2}} \right] - \frac{\hat{K}_{mn}}{2T} \\ \frac{\partial \hat{K}_{nn}}{\partial T} = & \frac{\pi}{\Lambda_d} \sqrt{\frac{\Lambda}{T}} f_n \sum_{m \neq n} \frac{\text{sgn}(\omega_m) f_m (|2m+1|(1-f_m) + (2n+1)(1-f_n))}{\sqrt{|n-m| + r/T}} - \frac{r}{2T^2} \sqrt{\frac{\Lambda}{T}} f_n \sum_{m \neq n} \frac{\text{sgn}(\omega_m) f_m}{(|n-m| + r/T)^{3/2}} \\ & - \frac{\hat{K}_{nn}}{2T} - \frac{\pi(2n+1)}{2T} - \frac{2\pi(2n+1)}{\Lambda_d} \sqrt{\frac{\Lambda}{T}} \frac{f_n^2(1-f_n)}{\sqrt{2n+1 + r/T}} + \frac{r}{2T^2} \sqrt{\frac{\Lambda}{T}} \frac{f_n^2}{(2n+1 + r/T)^{3/2}} \end{aligned} \quad (35)$$

Calculating these expressions, we present in Fig. III C $dT_c/d\tau_Q^{-1}$ in the proximity of a QCP. The results agree with our expectations and reveal that T_c is indeed in general more robust against disorder at the QCP ($r = 0$), specially when compared to the AG universal value $-\pi/4 \approx -0.785$. Although the precise values for T_c and $-dT_c/d\tau_Q^{-1}$ depend on the ratio Ω_c/Λ , the general trend is robust, and $-dT_c/d\tau_Q^{-1}$ remains well below the AG universal value $\pi/4$ as shown in Fig 1. To understand this behavior, we note that the last term of the Eliash-

berg equation (14), proportional to τ_Q^{-1} , effectively reduces the pairing vertex to $W_n \rightarrow W_n / \left(1 + \frac{\tau_Q^{-1}}{2Z_n|\omega_n|} \right)$. Therefore, because at the QCP the fermionic coherent weight $Z^{-1} \propto \omega^{1/2}$ vanishes at the Fermi surface, the effect of disorder on the pairing vertex becomes less relevant at low frequencies, where the gap function is the largest. As the system moves away from the QCP, Z^{-1} enhances at the Fermi level, and disorder becomes more relevant.

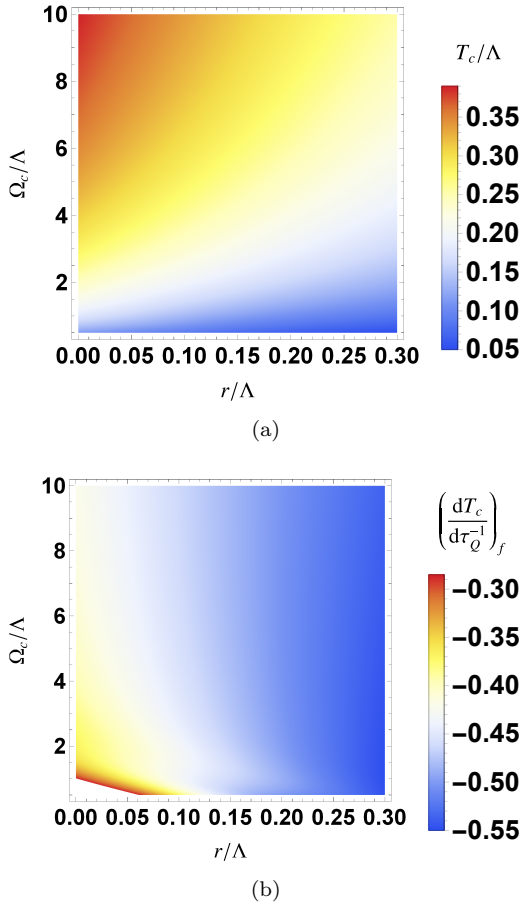


Figure 4. (a) Transition temperature of the clean system (T_c) as a function of the distance to the QCP r and the cutoff Ω_c (in units of the effective coupling Λ). (b) The suppression of T_c by disorder, $dT_c/d\tau^{-1}$, when the system is near the quantum critical point $r = 0$. Only the effects of the coupling of disorder to the fermionic degrees of freedom are included. In the plot, we used the soft cutoff procedure.

IV. SUPPRESSION OF T_c DUE TO THE COUPLING OF DISORDER AND BOSONIC DEGREES OF FREEDOM

Our analysis so far agrees with the general results from Ref.⁴⁶ and mirrors the standard AG approach for conventional dirty superconductors, with disorder impacting the electronic degrees of freedom. In this regard, one of the main differences between the conventional and unconventional SC cases stems from the reduced coherent electronic spectral weight near the QCP. There is however another important difference between the two cases: while in the former the pairing interaction arises from an independent degree of freedom (phonons), in the latter it arises from the same electronic degrees of freedom (AFM fluctuations). Since disorder affects the fermionic states, it must then change also the AFM fluctuation spectrum.

Within our functional approach to the Eliashberg equations, including this effect is straightforward within

linear order in τ^{-1} . Specifically, we need to compute how the pairing interaction, as defined in (9), changes in the presence of disorder. We identify two processes through which the bosonic degrees of freedom are affected by disorder scattering, as shown in Fig. IV (b) and (c) (see also Ref.⁴⁹). The first process, Fig. IV (b), corresponds to the renormalization of the electron-boson vertex by disorder, and gives rise to the contribution $(\frac{dT_c}{d\tau^{-1}})_{b,1}$ for the suppression of T_c . The second process, Fig. IV (c), corresponds to the renormalization of the bosonic self-energy, and gives rise to the contribution $(\frac{dT_c}{d\tau^{-1}})_{b,2}$. In the spirit of the large- N expansion, the renormalization of the disorder vertex by the bosonic fluctuations is small by a $1/N$ factor, and therefore will not be considered hereafter.

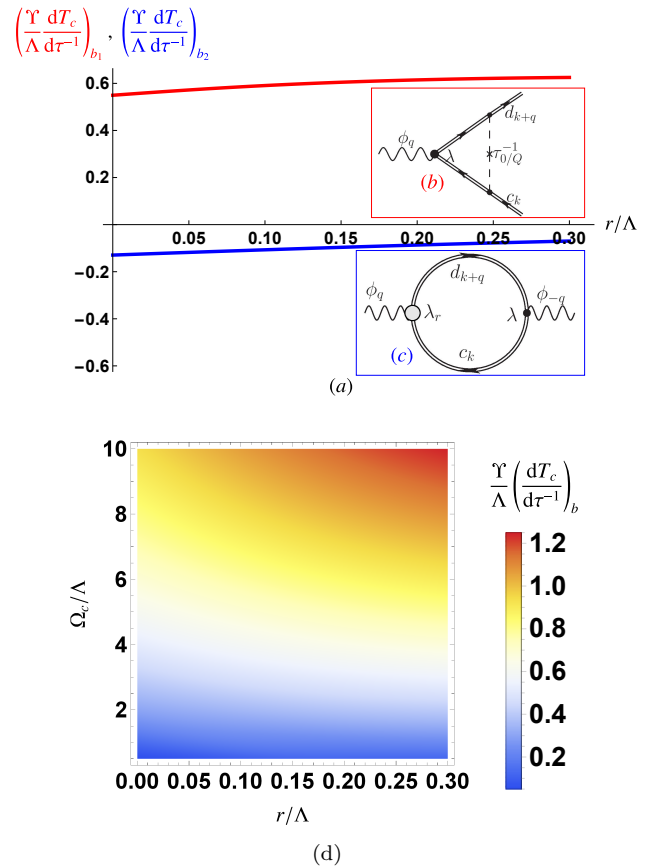


Figure 5. (a) Two contributions to the derivative of T_c with respect to the total scattering rate $\tau^{-1} = \tau_0^{-1} + \tau_Q^{-1}$ that arise from the coupling between disorder and bosonic degrees of freedom. The positive contribution b_1 corresponds to the dressing of the fermion-boson vertex by disorder (inset b), whereas the negative contribution b_2 corresponds to the dressing of the bosonic self-energy by disorder (inset c). (d) The change of T_c due to the coupling of disorder to the bosons, $(dT_c/d\tau^{-1})_b = (dT_c/d\tau^{-1})_{b,1} + (dT_c/d\tau^{-1})_{b,2}$, when the system is around the QCP $r = 0$.

A. Electron-boson vertex renormalization

We first calculate how the electron-boson vertex is renormalized by disorder. As shown in Fig. IV(b), the vertex correction $\delta\lambda$ is given by:

$$\begin{aligned} \delta\lambda &= n_{\text{imp}} u^2 \int \frac{d^2k}{(2\pi)^2} G_c \left(i\omega_n, \mathbf{k} - \frac{\mathbf{q}}{2} \right) G_d \left(i\omega_m, \mathbf{k} + \frac{\mathbf{q}}{2} + \mathbf{Q} \right) \\ &= \frac{n_{\text{imp}} u^2}{|\mathbf{v}_c \times \mathbf{v}_d|} \int \frac{d\epsilon_1 d\epsilon_2}{(2\pi)^2} \frac{1}{i\omega_n Z_n + \mathbf{v}_c \cdot \mathbf{q}/2 - \epsilon_1} \times \\ &\quad \frac{1}{i\omega_m Z_m - \mathbf{v}_c \cdot \mathbf{q}/2 - \epsilon_2} \end{aligned} \quad (36)$$

where n_{imp} is the impurity concentration and u is the impurity potential. Since the effect is the same for small and large momentum scattering, we do not distinguish them here. Using the result:

$$\int_{-\infty}^{\infty} \frac{dp}{ia - c - p} = -i\pi \text{sgn}(a). \quad (37)$$

we obtain:

$$\delta\lambda = -\lambda \frac{\text{sgn}(\omega_n \omega_m)}{8\pi N_f \tau |\mathbf{v}_c \times \mathbf{v}_d|}. \quad (38)$$

Note that the vertex correction depends only on the external frequencies of the two fermion legs. In the ladder approximation, we find the renormalized vertex λ_r

$$\begin{aligned} \lambda_r &= \lambda \left(1 + \frac{\text{sgn}(\omega_n \omega_m)}{8\pi N_f \tau |\mathbf{v}_c \times \mathbf{v}_d|} \right)^{-1} \\ \Rightarrow \left. \frac{d\lambda_r}{d\tau^{-1}} \right|_{\tau^{-1}=0} &= -\lambda \frac{\text{sgn}(\omega_n \omega_m)}{2\Upsilon}. \end{aligned} \quad (39)$$

where we defined the energy scale $\Upsilon = 4\pi N_f v_f^2 \sin\theta$. Thus, we have two different behaviors depending of whether the external frequencies have the same sign (λ_+) or different signs (λ_-)⁶³:

$$\lambda_{\pm} = \lambda \left(1 \pm \frac{1}{2\Upsilon\tau} \right)^{-1}, \quad \left. \frac{d\lambda_{\pm}}{d\tau^{-1}} \right|_{\tau^{-1}=0} = \mp \frac{\lambda}{2\Upsilon} \quad (40)$$

B. Bosonic self-energy renormalization

We now calculate the renormalization of the particle-hole bubble by disorder. As shown in Fig. IV(c), we have:

$$\begin{aligned} \Pi(i\Omega_m, \mathbf{q}) &= -2T \sum_n \int \frac{d^2q}{(2\pi)^2} \lambda_r \lambda G_c \left(i\omega_n, \mathbf{k} - \frac{\mathbf{q}}{2} \right) \\ &\quad \times G_d \left(i\omega_n + i\Omega_m, \mathbf{k} + \frac{\mathbf{q}}{2} + \mathbf{Q} \right) \\ &= \frac{\lambda^2}{2|\mathbf{v}_c \times \mathbf{v}_d|} T \sum_n \frac{\text{sgn}(\omega_m(\omega_m + \Omega_n))}{1 + \frac{1}{2\Upsilon\tau} \text{sgn}(\omega_m(\omega_m + \Omega_n))} \end{aligned} \quad (41)$$

Therefore, the particle-hole bubble does not depend on \mathbf{q} . In the static limit, we find:

$$\Pi(0) = \frac{\lambda^2 \Omega_c}{2\pi |\mathbf{v}_c \times \mathbf{v}_d|} \left(1 + \frac{1}{2\Upsilon\tau} \right)^{-1} \quad (42)$$

Thus, since the correlation length is given by $\xi^{-2} = r_0 - \chi_0 \Pi(0)$, and using the definition $r = \frac{\xi^{-2} \gamma}{2\pi}$, we find:

$$\frac{dr}{d\tau^{-1}} = \frac{\Omega_c}{4\pi\Upsilon} \quad (43)$$

The above result is consistent with previous works that found a reduction of the magnetic order parameter with disorder in itinerant AFM systems^{64,65}. We can also calculate the correction to the Landau damping $\gamma^{-1} \equiv \chi_0 [\Pi(0) - \Pi(i\Omega_n)] / |\Omega_n|$. We find:

$$\begin{aligned} \Pi(0) - \Pi(i\Omega_n) &= \frac{\lambda^2}{2|\mathbf{v}_c \times \mathbf{v}_d|} T \sum_{m=1}^{|\Omega_n|/(2\pi T)} \left[\left(1 + \frac{1}{2\Upsilon\tau} \right)^{-1} + \left(1 - \frac{1}{2\Upsilon\tau} \right)^{-1} \right] \\ &= \frac{\lambda^2 |\Omega_n|}{4\pi |\mathbf{v}_c \times \mathbf{v}_d|} \left[\left(1 + \frac{1}{2\Upsilon\tau} \right)^{-1} + \left(1 - \frac{1}{2\Upsilon\tau} \right)^{-1} \right] \end{aligned} \quad (44)$$

yielding:

$$\gamma^{-1} = \frac{\lambda^2 \chi_0}{2\pi |\mathbf{v}_c \times \mathbf{v}_d|} (1 - (2\Upsilon\tau)^{-2})^{-1}, \quad \frac{d\gamma^{-1}}{d\tau^{-1}} = 0 \quad (45)$$

Therefore, the Landau damping γ depends only quadratically on the scattering rate, and does not contribute to the leading order in τ^{-1} .

C. Total suppression rate of T_c

Using the results of the previous sections, we can rewrite the matrix elements in Eqs. (32 and 33) as:

$$\begin{aligned} \hat{K}_{m \neq n} &= \sqrt{\frac{\Lambda}{T}} \left(\frac{f_m f_n (\lambda_+/\lambda)^2}{\sqrt{|n-m|+r/T}} + \frac{f_m f_n (\lambda_-/\lambda)^2}{\sqrt{n+m+1+r/T}} \right) \\ \hat{K}_{nn} &= \frac{2(\lambda_-/\lambda)^2 f_n^2}{\sqrt{2n+1+r/T}} \sqrt{\frac{\Lambda}{T}} - \pi(2n+1) - \frac{1}{\tau_Q T} - \\ &\quad f_n \sqrt{\frac{\Lambda}{T}} \sum_{\substack{m \neq n \\ m=0}}^{N_c} f_m \left[\frac{(\lambda_+/\lambda)^2}{\sqrt{|n-m|+r/T}} - \frac{(\lambda_-/\lambda)^2}{\sqrt{n+m+1+r/T}} \right] \end{aligned} \quad (46)$$

While $\partial\eta/\partial T$ is the same as Eq. (35), the term $\partial\eta/\partial\tau^{-1}$ acquires two new contributions arising from the vertex renormalization (b_1) and from the self-energy renormalization (b_2):

$$\left(\frac{\partial\eta}{\partial\tau^{-1}} \right)_b = \left(\frac{\partial\eta}{\partial\tau^{-1}} \right)_{b,1} + \left(\frac{\partial\eta}{\partial\tau^{-1}} \right)_{b,2} \quad (47)$$

Using Eq. (40), we find the contribution from the vertex renormalization:

$$\begin{aligned} \Upsilon \left(\frac{\partial \hat{K}_{m \neq n}}{\partial \tau^{-1}} \right)_{b,1} &= \sqrt{\frac{\Lambda}{T}} f_m f_n \left[\frac{-1}{\sqrt{|n-m|+r/T}} \right. \\ &\quad \left. + \frac{1}{\sqrt{n+m+1+r/T}} \right] \\ \Upsilon \left(\frac{\partial \hat{K}_{nn}}{\partial \tau^{-1}} \right)_{b,1} &= 2f_n^2 \sqrt{\frac{\Lambda}{T}} (2n+1+r/T)^{-1/2} + \\ &\quad \sqrt{\frac{\Lambda}{T}} \sum_{\substack{m \neq n \\ m=0}} f_m f_n \left(\frac{1}{\sqrt{|n-m|+r/T}} + \frac{1}{\sqrt{n+m+1+r/T}} \right) \end{aligned} \quad (48)$$

Similarly, we find the contribution from the bosonic self-energy renormalization

$$\begin{aligned} \Upsilon \left(\frac{\partial \hat{K}_{m \neq n}}{\partial \tau^{-1}} \right)_{b,2} &= -f_m f_n \frac{\Omega_c}{8\pi T} \sqrt{\frac{\Lambda}{T}} \left[(|n-m|+r/T)^{-\frac{3}{2}} \right. \\ &\quad \left. + (n+m+1+r/T)^{-\frac{3}{2}} \right] \\ \Upsilon \left(\frac{\partial \hat{K}_{nn}}{\partial \tau^{-1}} \right)_{b,2} &= -2f_n^2 \frac{\Omega_c}{8\pi T} \sqrt{\frac{\Lambda}{T}} (2n+1+r/T)^{-\frac{3}{2}} + \\ &\quad \frac{\Omega_c}{8\pi T} \sqrt{\frac{\Lambda}{T}} \sum_{\substack{m \neq n \\ m=0}} f_m f_n \left[(|n-m|+r/T)^{-\frac{3}{2}} - \right. \\ &\quad \left. (n+m+1+r/T)^{-\frac{3}{2}} \right] \end{aligned} \quad (49)$$

It is now straightforward to compute $(\frac{dT_c}{d\tau^{-1}})_{b,1}$ and $(\frac{dT_c}{d\tau^{-1}})_{b,2}$ numerically, using the solution of the clean system obtained in the previous section. The red curve in Fig. IV(a) shows $(\frac{dT_c}{d\tau^{-1}})_{b,1}$ as function of the distance to the QCP, whereas the blue curve shows $(\frac{dT_c}{d\tau^{-1}})_{b,2}$. Surprisingly, not only the former is larger in magnitude than the latter, but it is also positive, whereas the latter is negative. The result $(\frac{dT_c}{d\tau^{-1}})_{b,2} < 0$ is straightforward to understand qualitatively: because $r \propto \xi^{-2}$ is enhanced by disorder, according to Eq. (43), the system behaves as it moves away from the QCP, which effectively reduces T_c , according to the behavior found previously in the clean system in Fig. 1. On the other hand, the result $(\frac{dT_c}{d\tau^{-1}})_{b,2} > 0$ is less straightforward to understand qualitatively, particularly since disorder may enhance or suppress the vertex λ depending on the frequencies of the two external fermions, as shown by Eq. (40).

This unexpected result can be understood by analyzing the expression for the coherent spectral weight Z_n^{-1} , Eq. (13), in the presence of the renormalized electron-boson coupling λ_r (and in the absence of other impurity terms). At the QCP, we find that at low frequencies, $\omega \ll \Lambda_c$, Z_n is effectively reduced by this vertex renor-

malization, $(\frac{dZ}{d\tau^{-1}})_{b,1} = -\frac{1}{\Upsilon[\omega]} \sqrt{\frac{\Lambda \Omega_c}{2\pi}}$. Consequently, because Z_n appears in the denominator of the pairing kernel in the gap equation (14), the SC transition temperature is enhanced by this effect. Note that the pairing kernel also has a factor of λ^2 in the numerator; however, because the sign of the vertex correction $\delta\lambda$ in Eq. (38) changes depending on the relative frequencies of the external fermions, it does not compensate for the effect arising from the suppression of Z_n in the denominator. Indeed, the only reason Z_n is efficiently suppressed by λ^2 is because of the term $\text{sign}(\omega_m)$ inside the sum in Eq. (13), which is compensated by the same term $\text{sign}(\omega_m)$ in Eq. (39). Such compensation leads to the cutoff dependence of $dZ/d\tau^{-1}$, and outweighs the impact of disorder on the renormalized pairing kernel.

Analytically, we can obtain approximate expressions for both $(\frac{dT_c}{d\tau^{-1}})_{b,1}$ and $(\frac{dT_c}{d\tau^{-1}})_{b,2}$ at the QCP, $r = 0$. The details are shown in Appendix A, and give:

$$\begin{aligned} \frac{\Upsilon}{\Lambda} \left(\frac{dT_c}{d\tau^{-1}} \right)_{b,1} &\approx 0.6 \sqrt{\frac{\Omega_c}{\Lambda}} \\ \frac{\Upsilon}{\Lambda} \left(\frac{dT_c}{d\tau^{-1}} \right)_{b,2} &\approx -0.045 \frac{\Omega_c}{\Lambda} \end{aligned} \quad (50)$$

The reason why $(\frac{dT_c}{d\tau^{-1}})_{b,2}$ grows faster with Ω_c is because high-energy states contribute more to the particle-hole bubble than to the vertex correction. In Fig. IV(d) we present the net result $\frac{\Upsilon}{\Lambda} (\frac{dT_c}{d\tau^{-1}})_{b,1} + \frac{\Upsilon}{\Lambda} (\frac{dT_c}{d\tau^{-1}})_{b,2}$ as function of the distance to the QCP and of the cutoff. Clearly, for a wide regime of parameters the net effect of the coupling between disorder and bosonic degrees of freedom is an enhancement of T_c .

V. CONCLUDING REMARKS

In this work, we used a variational approach to investigate how different effects contribute to the suppression rate of T_c by disorder, $\frac{dT_c}{d\tau^{-1}}$, in the case of an unconventional superconductor in which pairing is mediated by quantum critical fluctuations. By studying the spin-fermion model in the large- N hot-spot approximation, we identified three different contributions to the reduction of T_c with impurity scattering, $\frac{dT_c}{d\tau^{-1}} = (\frac{dT_c}{d\tau^{-1}})_f + (\frac{dT_c}{d\tau^{-1}})_{b,1} + (\frac{dT_c}{d\tau^{-1}})_{b,2}$, as outlined in Eq. (1). $(\frac{dT_c}{d\tau^{-1}})_f$ arises from the pair-breaking effect promoted by the coupling between the electrons and the large-momentum impurity potential. As shown in Fig. III C, $(\frac{dT_c}{d\tau^{-1}})_f$ is always negative albeit reduced with respect to the Abrikosov-Gor'kov value near the QCP. Such a reduction stems from the suppression of quasi-particle spectral weight near the QCP, and has its roots on the non-Fermi liquid character of the AFM QCP.

While this trend agrees with results from previous works on similar spin-fermion models^{46,53}, our variational

approach, by means of the Hellmann-Feynman theorem, allows us to also assess the effect of the coupling between disorder and the pairing interaction (i.e. the bosonic degrees of freedom) without having to solve the complicated disordered problem. Two contributions arise: $(\frac{dT_c}{d\tau^{-1}})_{b,1}$, due to the dressing of the electron-boson vertex by impurities, and $(\frac{dT_c}{d\tau^{-1}})_{b,2}$ due to the dressing of the bosonic self-energy by impurities. Surprisingly, we find $(\frac{dT_c}{d\tau^{-1}})_{b,1} > 0$ close to the QCP and larger in magnitude than $(\frac{dT_c}{d\tau^{-1}})_{b,2} < 0$. While the latter behavior can be understood as a result of the suppression of the magnetic correlation length by disorder, the former stems from the enhancement of the quasi-particle spectral weight promoted by the renormalization of the electron-boson coupling.

It is interesting to discuss the relative magnitudes of these effects. Our analytical approximations, combined with the numerical results, show that at the QCP the two effects arising from the coupling of disorder to the bosons behave as $|\frac{dT_c}{d\tau^{-1}}|_{b,2} \sim \frac{0.04}{\sin \theta} |\frac{dT_c}{d\tau^{-1}}|_{b,1}$. Therefore, unless the system is very close to perfect nesting ($\theta = 0$), the positive contribution $(\frac{dT_c}{d\tau^{-1}})_{b,1}$ overcomes the negative contribution $(\frac{dT_c}{d\tau^{-1}})_{b,2}$, as illustrated in Fig. IV(d). Consequently, the suppression rate of T_c enforced by the direct coupling of the fermions to the impurity potential $(\frac{dT_c}{d\tau^{-1}})_f$ is even more reduced as compared to the Abrikosov-Gor'kov value. In particular, we can estimate using our analytical expressions $|\frac{dT_c}{d\tau^{-1}}|_{b,1} \sim \frac{\lambda^2 \chi_0}{E_F} |\frac{dT_c}{d\tau^{-1}}|_f$, implying that this additional enhancement of T_c is generally smaller than the reduction promoted by pair-breaking effects. Equivalently, within an expansion in the number of hot spots N , this additional contribution acquires a prefactor of $1/\sqrt{N}$. Thus, the universal value

$\left(\frac{dT_c}{d\tau^{-1}}\right)_f \approx -0.45$ obtained at the QCP (i.e. the value obtained when $r = 0$ and $\Omega_c \rightarrow \infty$) is an upper boundary value that may in principle be used to test this model. Experimentally, it would be interesting to obtain $(\frac{dT_c}{d\tau^{-1}})$ experimentally in electron-doped cuprates or iron pnictides near the putative AFM QCP by introducing disorder in a controlled way via, for instance, irradiation.

In summary, we have shown that the suppression of T_c by weak disorder in an AFM quantum critical SC is significantly reduced compared to the universal value obtained from the Abrikosov-Gor'kov theory of conventional dirty SC. Our work highlights the importance of the incoherent electronic spectral weight and of the feedback of the electronic states on the pairing interaction to describe the properties of this unconventional pairing state. Qualitatively, our results agree with several experimental observations in cuprates and pnictides reporting a robust SC state against disorder. Extensions of this promising framework to include higher-order contributions from the impurity scattering would be desirable to achieve more quantitative comparisons with experiments, such as the critical value of the impurity scattering that destroys the quantum critical SC state.

ACKNOWLEDGMENTS

We thank A. Chubukov, A. Millis, J. Schmalian, X. Wang, and Y. Wang for fruitful discussions. This work was supported by the U.S. Department of Energy, Office of Science, Basic Energy Sciences, under award number de-sc0012336.

* jkang@umn.edu

- ¹ F. Steglich, J. Aarts, C.D. Bredl, W. Lieke, D. Meschede, W. Franz, and H. Schafer, Phys. Rev. Lett. **43**, 1892 (1979).
- ² G.R. Stewart, Z. Fisk, J.O. Willis, and J.L. Smith, Phys. Rev. Lett. **52**, 679 (1984).
- ³ D. Jerome, A. Mazaud, M. Ribault, and K. Bechgaard. J. Phys. (Paris) Lett. **41** L95, 1980.
- ⁴ S. M. De Soto, C. P. Slichter, A. M. Kini, H. H. Wang, U. Geiser, and J. M. Williams, Phys. Rev. B **52**, 10364 (1995).
- ⁵ J. G. Bednorz and K. A. Muller, Z. Phys. B **64**, 189 (1986).
- ⁶ Y. Kamihara, T. Watanabe, M. Hirano, and H. Hosono, J. Am. Chem. Soc. **130**, 3296 (2008).
- ⁷ J.E. Hirsch, Phys. Rev. Lett. **54**, 1317 (1985).
- ⁸ K. Miyake, S. Schmitt-Rink, and C.M.Varma, Phys. Rev. B **34**, 6554 (1986).
- ⁹ A.J. Millis, S. Sachdev, and C.M.Varma, Phys. Rev. B **37**, 4975 (1988).
- ¹⁰ D.J. Scalapino, E. Loh, Jr. and J.E. Hirsch, Phys. Rev. B **34**, 8190 (1986).

- ¹¹ D.A. Wollman, D.J. Van Harlingen, W.C. Lee, D.M. Ginsberg, and A.J. Leggett, Phys. Rev. Lett. **71**, 2134 (1993).
- ¹² D. J Van Harlingen, Physica C **282-287**, 128 (1997).
- ¹³ C.C. Tsuei, J.R. Kirtley, C.C. Chi, Lock See Yu-Jahnes, A. Gupta, T. Shaw, J.Z. Sun, and M.B. Ketchen, Phys. Rev. Lett. **73**, 593 (1994).
- ¹⁴ P. Monthoux and D. Pines, Phys. Rev. Lett. **69**, 961 (1992).
- ¹⁵ P. Monthoux, D. Pines, and G. G. Lonzarich, Nature, **450**, 1177 (2007).
- ¹⁶ I. I. Mazin, D. J. Singh, M. D. Johannes, and M. H. Du, Phys. Rev. Lett. **101**, 057003 (2008).
- ¹⁷ K. Kuroki, S. Onari, R. Arita, H. Usui, Y. Tanaka, H. Kontani, and H. Aoki. Phys. Rev. Lett. **101**, 087004 (2008).
- ¹⁸ P.J. Hirschfeld, M. M. Korshunov, and I. I. Mazin, Rep. Prog. Phys. **74**, 124508 (2011).
- ¹⁹ D. J. Scalapino, Rev. Mod. Phys. **84**, 1383 (2012).
- ²⁰ A. V. Chubukov, Annu. Rev. Cond. Mat. Phys. **3**, 57 (2012).
- ²¹ T. Valla, A. V. Fedorov, P. D. Johnson, B. O. Wells, S. L. Hulbert, Q. Li, G. D. Gu, and N. Koshizuka, Science **285**

- 2110 (1999).
- 22 S. Jiang, H. Xing, G. Xuan, C. Wang, Z. Ren, C. Feng, J. Dai, Z. Xu and G. Cao, *Journal of Physics: Condensed Matter* **21**, 382203 (2009).
 - 23 T. Shibauchi, A. Carrington, and Y. Matsuda, *Annu. Rev. Condens. Matter Phys.* **5**, 113 (2014).
 - 24 S. Sachdev, *Quantum Phase Transitions* (Cambridge University Press, Cambridge, England, 2001).
 - 25 A. Abanov, A.V. Chubukov and A.M. Finkel'stein, *Europhys. Lett.* **54**, 488 (1999).
 - 26 A. Abanov, A. V. Chubukov, and J. Schmalian. *Adv. Phys.* **52**, 119 (2003).
 - 27 M. A. Metlitski, and S. Sachdev, *Phys. Rev. B* **82**, 075127 (2010); *Phys. Rev. B* **82**, 075128 (2010).
 - 28 E. Berg, M. A. Metlitski, and S. Sachdev, *Science* **338**, 1606 (2012).
 - 29 M. A. Metlitski, D. F. Mross, S. Sachdev, and T. Senthil, *Phys. Rev. B* **91**, 115111 (2015).
 - 30 J.-H. She, B. J. Overbosch, Y.-W. Sun, Y. Liu, K. E. Schalm, J. A. Mydosh, and J. Zaanen, *Phys. Rev. B* **84**, 144527 (2011).
 - 31 Y. Wang and A. V. Chubukov, *Phys. Rev. Lett.* **110**, 127001 (2013).
 - 32 S. Raghu, G. Torroba, and H. Wang, arXiv:1507.06652.
 - 33 Y. Schattner, S. Lederer, S. A. Kivelson, and E. Berg, arXiv:1511.03282.
 - 34 K. B. Efetov, H. Meier, and C. Pépin, *Nat. Phys.* **9**, 442 (2013).
 - 35 A. V. Balatsky, I. Vekhter, and J.-X. Zhu, *Rev. Mod. Phys.* **78**, 373 (2006).
 - 36 P. W. Anderson, *J. Phys. Chem. Solids* **11**, 26 (1959).
 - 37 A. A. Abrikosov and L. P. Gor'kov, *Sov. Phys. JET* **12**, 1243 (1961).
 - 38 M. A. Woolf and F. Reif, *Phys. Rev.* **137**, A557 (1965).
 - 39 S. K. Tolpygo, J.-Y. Lin, M. Gurvitch, S. Y. Hou, and J. M. Phillips, *Phys. Rev. B* **53**, 12454 (1996).
 - 40 K. Kirshenbaum, S. R. Saha, S. Ziemak, T. Drye, and J. Paglione, *Phys. Rev. B* **86**, 140505 (2012).
 - 41 H. Alloul, J. Bobroff, M. Gabay, and P. J. Hirschfeld, *Rev. Mod. Phys.* **81**, 45 (2009).
 - 42 K. Fujita, T. Noda, K. M. Kojima, H. Eisaki, and S. Uchida, *Phys. Rev. Lett.* **95**, 097006 (2005).
 - 43 Y. Nakajima, T. Taen, Y. Tsuchiya, T. Tamegai, H. Kitamura, and T. Murakami, *Phys. Rev. B* **82**, 220504 (2010).
 - 44 F. Rullier-Albenque, H. Alloul, and R. Tourbot, *Phys. Rev. Lett.* **91**, 047001 (2003).
 - 45 A. F. Kemper, D. G. S. P. Doluweera, T. A. Maier, M. Jarrell, P. J. Hirschfeld, and H-P. Cheng, *Phys. Rev. B* **79**, 104502 (2009).
 - 46 A. B. Vorontsov, A. Abanov, M. G. Vavilov, and A. V. Chubukov, *Phys. Rev. B* **81**, 012508 (2010).
 - 47 Y. Wang, A. Kreisel, P. J. Hirschfeld, and V. Mishra, *Phys. Rev. B* **87**, 094504 (2013).
 - 48 Y. Yamakawa, S. Onari, and H. Kontani, *Phys. Rev. B* **87**, 195121 (2013).
 - 49 F. Palestini and G. C. Strinati, *Phys. Rev. B* **88**, 174504 (2013).
 - 50 H. Chen, Y.-Y. Tai, C. S. Ting, M. J. Graf, J. Dai, J.-X. Zhu, *Phys. Rev. B* **88**, 184509 (2013).
 - 51 M. S. Scheurer, M. Hoyer, J. Schmalian, *Phys. Rev. B* **92**, 014518 (2015).
 - 52 A. Garg, M. Randeria, and N. Trivedi, *Nature Physics* **4**, 762 (2008).
 - 53 R. J. Radtke, K. Levin, H.-B. Schuttler, and M. R. Norman, *Phys. Rev. B* **48**, 653 (1993).
 - 54 M. Franz, C. Kallin, A. J. Berlinsky, and M. I. Salkola, *Phys. Rev. B* **56**, 7882 (1997).
 - 55 S. Tang, V. Dobrosavljevic, and E. Miranda, arXiv:1510.08152.
 - 56 S. Onari and H. Kontani, *Phys. Rev. Lett.* **103**, 177001 (2009).
 - 57 G. M. Eliashberg, *Sov. Phys. JETP* **11**, 696 (1960); *Sov. Phys. JETP* **16**, 780 (1963).
 - 58 D. J. Bergmann and D. Rainer, *Z. Phys.* **263**, 59 (1973).
 - 59 R. M. Fernandes and A. J. Millis, *Phys. Rev. Lett.* **110**, 117004 (2013).
 - 60 K. Levin and O. T. Valls, *Phys. Rev. B*, **17**, 191 (1978).
 - 61 I. Martin, D. Podolsky, and S. A. Kivelson, *Phys. Rev. B* **72**, 060502(R) (2005).
 - 62 A. T. Romer, S. Graser, T. S. Nunner, P. J. Hirschfeld, and B. M. Andersen, *Phys. Rev. B* **86**, 054507 (2012).
 - 63 S. V. Syzranov and J. Schmalian, *Phys. Rev. Lett.* **109**, 156403 (2012).
 - 64 R. M. Fernandes, M. G. Vavilov, and A. V. Chubukov, *Phys. Rev. B* **85**, 140512(R) (2012).
 - 65 S. Liang, C. B. Bishop, A. Moreo, and E. Dagotto, *Phys. Rev. B* **92**, 104512 (2015).
 - 66 S. Sur and S.-S. Lee, *Phys. Rev. B* **91**, 125136 (2015).
 - 67 S. A. Maier and P. Strack, *Phys. Rev. B* **93**, 165114 (2016).

Appendix A: analytical calculation of $\left(\frac{dT_c}{d\tau^{-1}}\right)_{b,1}$ and $\left(\frac{dT_c}{d\tau^{-1}}\right)_{b,2}$ at the QCP

Here we focus on the case where the system is at the QCP, $r = 0$, and apply the hard cutoff procedure for $N_c \gg 1$. We start by computing $\left(\frac{dT_c}{d\tau^{-1}}\right)_{b,1}$. In this case, the expressions (48) simplify to:

$$\begin{aligned} \Upsilon \left(\frac{\partial K_{nn}}{\partial \tau^{-1}} \right)_{b,1} &= \sqrt{\frac{\Lambda}{T}} \left[2\zeta \left(\frac{1}{2}, 1 \right) - \zeta \left(\frac{1}{2}, N_c - n \right) \right. \\ &\quad \left. - \zeta \left(\frac{1}{2}, N_c + n \right) + \frac{1}{\sqrt{2n+1}} \right] \\ \Upsilon \left(\frac{\partial K_{m \neq n}}{\partial \tau^{-1}} \right)_{b,1} &= -\sqrt{\frac{\Lambda}{T}} \left[\frac{1}{\sqrt{|m-n|}} - \frac{1}{\sqrt{m+n+1}} \right] \end{aligned} \quad (S1)$$

where $\zeta(a, x)$ is the Hurwitz zeta function. In the limit $N_c \gg 1$, the off-diagonal term is much smaller than the diagonal one. Consequently, the change in the eigenvalue is given by:

$$\Upsilon \sqrt{\frac{T}{\Lambda}} \left(\frac{d\eta}{d\tau^{-1}} \right)_{b,1} = 2 \sum_{n=0}^{N_c} \bar{\Delta}_n^2 \left(\sqrt{N_c - n} + \sqrt{N_c + n} \right) \quad (S2)$$

where the eigenvectors are normalized, $\sum_n \bar{\Delta}_n^2 = 1$. As discussed in the solution of the clean case, $\bar{\Delta}_{n \geq n_0} \approx A n^{-3/2}$ for $1 \ll n_0 \ll N_c$, with $A > 0$. Thus, we ob-

tain:

$$\begin{aligned} \Upsilon \sqrt{\frac{T}{\Lambda}} \left(\frac{d\eta}{d\tau^{-1}} \right)_{b,1} &\approx 4\sqrt{N_c} \sum_{n=0}^{n_0} \bar{\Delta}_n^2 \\ &+ 2A^2 \int_{n_0}^{N_c} dn \left(\frac{\sqrt{N_c - n} + \sqrt{N_c + n}}{n^3} \right) \\ &\approx 4\sqrt{N_c} \sum_{n=0}^{n_0} \bar{\Delta}_n^2 + \frac{2A^2 \sqrt{N_c}}{n_0^2} \end{aligned} \quad (\text{S3})$$

yielding:

$$\Upsilon \left(\frac{d\eta}{d\tau^{-1}} \right)_{b,1} \approx \frac{8}{\sqrt{2\pi}} \sqrt{\frac{\Omega_c}{\Lambda}}. \quad (\text{S4})$$

where we used the clean limit result $T_c \approx \Lambda/2$. Therefore, T_c actually increases due to the dressing of the fermion-boson vertex by disorder. To evaluate the change in T_c due to this effect, we use Eq. (30):

$$- \left(\frac{dT_c}{dT} \right) = - \frac{\pi}{2T} \sum_{n=0}^{\infty} \bar{\Delta}_n^2 (2n+1) \approx \frac{1.6\pi}{\Lambda} \quad (\text{S5})$$

where the last step was obtained by the numerical solution of the clean system at the QCP. Therefore, we obtain:

$$\frac{\Upsilon}{\Lambda} \left(\frac{dT_c}{d\tau^{-1}} \right)_{b,1} \approx 0.6 \sqrt{\frac{\Omega_c}{\Lambda}} \quad (\text{S6})$$

This approximate analytical expression is in very good agreement with the numerical results, as shown in Fig. S1(a).

We now move on to compute $\left(\frac{dT_c}{d\tau^{-1}} \right)_{b,2}$ at the QCP. From Eq. (49) we have, for $r = 0$:

$$\begin{aligned} \Upsilon \left(\frac{\partial \hat{K}_{nn}}{\partial \tau^{-1}} \right)_{b,2} &= \frac{\Omega_c}{4\pi T} \sqrt{\frac{\Lambda}{T}} \left[\zeta \left(\frac{3}{2}, 1 \right) - \zeta \left(\frac{3}{2}, n+1 \right) \right. \\ &\quad \left. - \frac{1}{2(2n+1)^{3/2}} \right] \\ \Upsilon \left(\frac{\partial \hat{K}_{m \neq n}}{\partial \tau^{-1}} \right)_{b,2} &= - \frac{1}{2} \frac{\Omega_c}{4\pi T} \sqrt{\frac{\Lambda}{T}} \left[\frac{1}{|m-n|^{3/2}} + \right. \\ &\quad \left. \frac{1}{(m+n+1)^{3/2}} \right] \end{aligned} \quad (\text{S7})$$

As a result, using the same procedure as above, we obtain:

$$\begin{aligned} \Upsilon \sqrt{\frac{T}{\Lambda}} \frac{4\pi T}{\Omega_c} \left(\frac{d\eta}{d\tau^{-1}} \right)_{b,2} &= \sum_n \bar{\Delta}_n^2 \left[\zeta \left(\frac{3}{2}, 1 \right) - \zeta \left(\frac{3}{2}, n+1 \right) \right] \\ &- \frac{1}{2} \sum_{m,n} \bar{\Delta}_m \bar{\Delta}_n \left[\frac{1 - \delta_{mn}}{|m-n|^{3/2}} + \frac{1}{(m+n+1)^{3/2}} \right] \end{aligned} \quad (\text{S8})$$

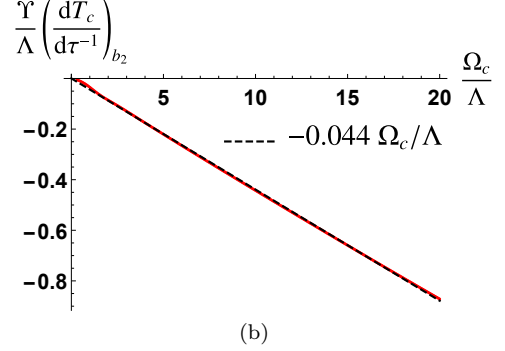
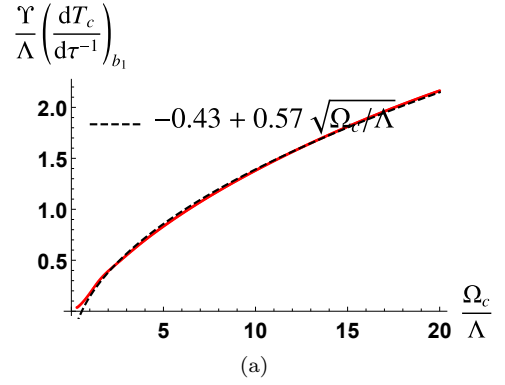


Figure S1. Contribution to the suppression rate $(dT_c/d\tau^{-1})$ arising from the impurity dressing of (a) the fermion-boson coupling and (b) the bosonic self-energy. Solid curves are the numerical result, dashed curves are the analytical approximations.

Using the numerical solution of the clean system at the QCP, we find for the right-hand side of the equation:

$$\Upsilon \sqrt{\frac{T}{\Lambda}} \frac{4\pi T}{\Omega_c} \left(\frac{d\eta}{d\tau^{-1}} \right)_{b,2} \approx -1 \quad (\text{S9})$$

yielding:

$$\frac{\Upsilon}{\Lambda} \left(\frac{dT_c}{d\tau^{-1}} \right)_{b,2} \approx -0.045 \frac{\Omega_c}{\Lambda} \quad (\text{S10})$$

As shown in Fig. S1(b), the numerical results agree well with this expression.